

Received: 2020.03.27

Accepted: 2020.05.27

Available online: 2020.07.31

Published: 2020.09.21

# Construction and Evaluation of Folic Acid-Modified 3-Bromopyruvate Cubosomes

**Authors' Contribution:**

Study Design A  
Data Collection B  
Statistical Analysis C  
Data Interpretation D  
Manuscript Preparation E  
Literature Search F  
Funds Collection G

**ABCDEF 1 Fangyan Hou**  
**BF 1 Hairong Wang**  
**CF 1 Yawen Zhang**  
**ACF 2 Na Zhu**  
**ACDG 1 Hao Liu**  
**ACDEG 1 Jianchun Li**

1 School of Pharmacy, Bengbu Medical College, Bengbu, Anhui, P.R. China  
2 Tianjin Key Laboratory of Biomedical Materials, Institute of Biomedical Engineering, Chinese Academy of Medical Sciences and Peking Union Medical College, Tianjin, P.R. China

**Corresponding Authors:**

Hao Liu, e-mail: [liuhao6886@foxmail.com](mailto:liuhao6886@foxmail.com), Jianchun Li, e-mail: [lijc66577@sohu.com](mailto:lijc66577@sohu.com)

**Source of support:**

This work was supported by The Key Program of Anhui University Natural Science Research [KJ2018A0998]

**Background:**

Direct 3-bromopyruvate chemotherapy often causes side effects. We thus aimed to construct and evaluate folic acid-modified 3-bromopyruvate liquid crystalline nanoparticles (3BP-LCNP-FA) and assess their targeted anti-tumor effects in tumor-bearing nude mice.

**Material/Methods:**

A liquid crystalline nanoparticle formulation was screened, and the structure was characterized using polarizing light- and transmission electron microscopy. The folate target was then synthesized and characterized using differential scanning calorimetry and proton nuclear magnetic resonance spectroscopy. *In vitro*, human CNE-2Z and MDA-MB-231 tumor cells were used to evaluate 3BP-LCNP-FA effects on tumor cell morphology and proliferation. Different drug formulations were administered to tumor-bearing nude mice to observe the treatment effects. Hepatic and renal toxicities were assessed using hematoxylin and eosin-stained liver, kidney, and lung sections along with serological analysis of liver and kidney injury markers (e.g., aspartate aminotransferase, alanine transaminase, blood urea nitrogen, and creatinine). Tumor tissue was observed for changes using proliferating cell nuclear antigen immunohistochemistry and terminal deoxynucleotidyl transferase dUTP nick end labeling assay.

**Results:**

We successfully prepared 3BP-LCNP-FA of spherical shape with uniform size using the aforementioned techniques; drug loading did not alter crystal morphology. These cubosomes exhibited more potent antitumor activity than 3-bromopyruvate alone or non-folic acid-conjugated 3-bromopyruvate liquid crystalline nanoparticles *in vitro* and *in vivo* without obvious toxic side effects.

**Conclusions:**


It is possible to successfully construct 3BP-LCNP-FA as a drug delivery vehicle that is more efficacious than 3-bromopyruvate and has no obvious toxic effects. Thus, folic acid-modified cubosomes can be used as effective carriers for targeted drug administration.

**MeSH Keywords:**

**Antineoplastic Agents • Drug Delivery Systems • Folic Acid • Nanoparticles**

**Full-text PDF:**

<https://www.medscimonit.com/abstract/index/idArt/924620>

 3540

 1

 11

 32



## Background

Modern antitumor treatments are expected to minimize damage to non-target organs by improving drug targeting. In particular, the highly active aerobic glycolysis in a variety of tumor cells acts as a potential target for modern antitumor therapies [1,2]. As one such therapeutic agent, 3-bromopyruvate (3BP) inhibits glycolysis, consequently limiting energy supply to tumor cells and inhibiting their rapid proliferation [3–7]. Studies have found that 3BP enters tumor cells through monocarboxylic acid transporter 1 (MCT1) present on the cell membrane surface [8,9], inhibits the activity of hexokinase II bound to the outer membrane of mitochondria, and consequently limits energy production in cells and inhibits their rapid growth [10–14]. Therefore, the therapeutic effect of 3BP is poor in tumor cells with low MCT1 expression [15]. Moreover, clinical application of 3BP has been associated with side effects as this agent interacts with healthy cells, particularly erythrocytes, reducing its availability to tumor cells and narrowing its therapeutic window [16–20].

Alternatively, previous studies have shown that several folate receptors (FRs) are highly expressed on the surface of some tumor cells, especially those exhibiting rapid growth [21,22], and therefore, they can be used as therapeutic targets. Accordingly, modifying the FR ligand, folic acid (FA), to accommodate 3BP can increase the selectivity potential of a drug carrier system incorporated with 3BP. Moreover, active drug targeting to the desired organs or cells through FR mediation further improves drug targeting and reduces side effects, as this allows for active targeted transport of the FA-drug conjugate by endocytosis [23]. Once the FA-drug conjugate enters the cell, the pH of endocytosomes (pH 5), in contrast to that of the extracellular space (pH 7), leads to altered conformation of the drug and FR complexes. The folate conjugate can then separate from the FR, enter the cytoplasm, and exert its therapeutic effects, whereas the FR can return to the cell surface and continue to transport drugs. Thus, an FR-mediated, active drug delivery system targets tumor sites in two ways: direct coupling of FA to drug molecules and FA coupling to the drug carrier surface. However, as coupling of FA to drug molecules can further reduce drug solubility, research has primarily focused on FA coupled to the surface of drug carriers [24,25]. In addition, current FA-targeted drug delivery systems have mostly been evaluated using *in vitro* toxicity tests. Few experimental data are available in animals with the targeted therapeutic effects in humans also requiring further study.

Liquid crystalline nanoparticles [26] (LCNPs) are self-assembled, bi-continuous liquid crystalline phases comprising a lipid bilayer enclosing water channels, which provides both a hydrophilic and hydrophobic region for encapsulation of drugs with varying solubilities [27–29]. These liquid crystals can be lamellar, hexagonal, or cubic (cubosomes). Owing to their unique reverse

bi-continuous cubic phase structure, cubosomes do not cause the side effects that are associated with nude drug administration, such as burning sensation in the veins, rapid blood-based clearance, and off-target side effects. Conversely, cubosomes are highly biocompatible and bioadhesive and can be administered via different routes [30]. In addition, LCNPs can enter the cell through endocytosis, which does not depend on presence of MCT1 transporters on the cell membrane surface, enabling transport of the drug into tumor cells to a greater extent. Some of the currently researched dosage forms of 3BP include liposomes, gold NPs, and microencapsulation. However, there are no data in the literature on FA-modified cubic liquid crystalline nanoparticles. In addition, most of the studies on cubosomes are based on *in vitro* laboratory research, and there is a lack of *in vivo* research data.

Given the excellent drug delivery performance of cubosomes and tumor-targeting effects of drug modification with FA, we hypothesized that FA-modified 3BP cubosomes (3BP-LCNP-FA) would not be dependent on cell surface MCT1 proteins for intracellular transport and may show improved antitumor effects without the toxic effects that are typically associated with 3BP treatment. Therefore, in this study, we constructed 3BP-LCNP-FA and evaluated *in vitro* antitumor effects in CNE-2Z cells with high MCT1 expression on the surface of tumor cell membrane and MDA-MB-231 2 cells with low MCT1 expression. *In vivo* antitumor effects were evaluated in tumor bearing nude mice (Figure 1).

## Material and Methods

### Chemicals

We acquired 3BP from Sigma Co. Ltd. (Shanghai, China). Glycerol monooleate (GMO) was purchased from Baoman Co. Ltd. (Shanghai, China). Poloxamer 407 (F127), FA, and 1,1-carbonyldiimidazole (CDI) were provided by Yuan Ye Co. Ltd. (Shanghai, China). An adenosine triphosphate (ATP) measurement kit was purchased from Beyotime Biotechnology (S0026, Shanghai, China). Dialysis bags with a molecular weight cutoff of 3500 Da (Viskase Companies, Inc., Darien, IL, USA) were used. RPMI 1640 and Dulbecco's modified Eagle's medium were acquired from Thermo Fisher Biochemical Products (Beijing, China). Fetal bovine serum was supplied by Tian Hang Biotechnology Co. Ltd. (Hangzhou, China). The CNE-2Z and MDA-MB-231 human tumor cell lines were supplied by the biochemical laboratory of Nanjing University.

### Cell culture and animals

The human tumor cell lines CNE-2Z and MDA-MB-231, representing high- and low MCT expression, respectively, were used

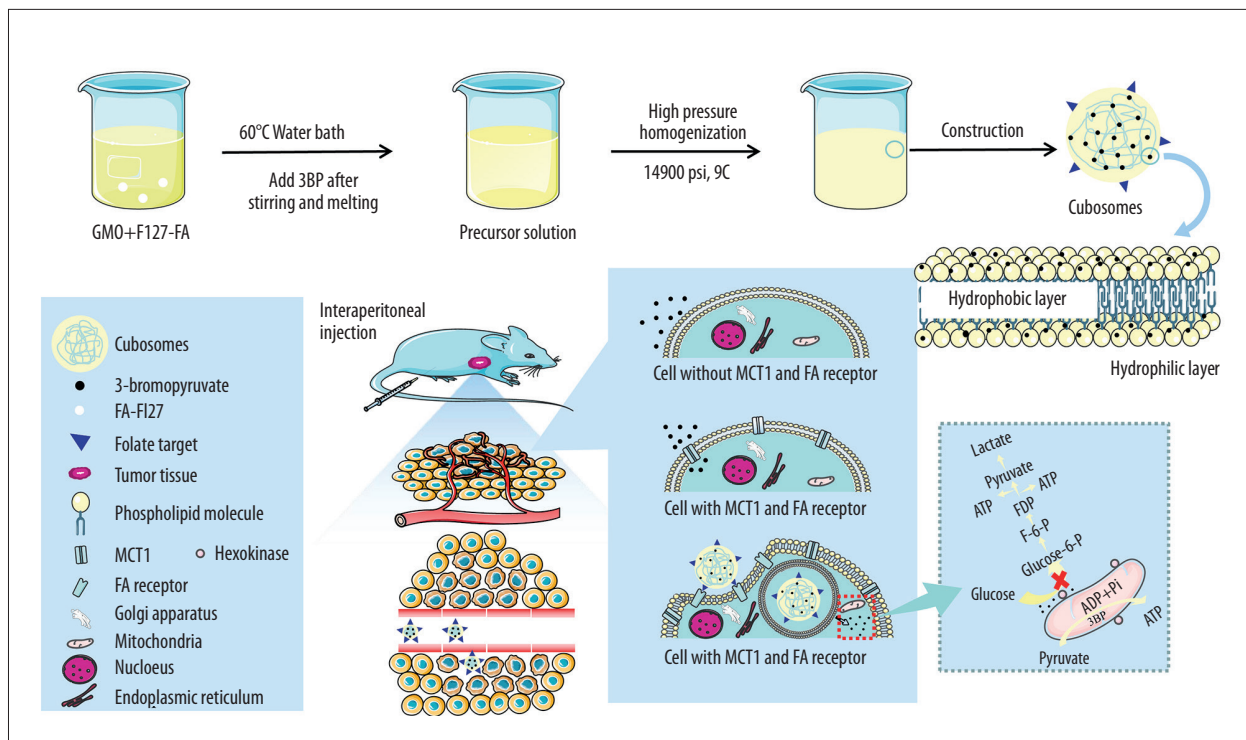


**Figure 1.** Construction and mechanism of 3BP-LCNP-FA. Synthetic process and structure of 3BP-LCNP-FA. 3-bromopyruvate is a hydrophilic drug and located in the hydrophilic segment of the phospholipid bilayer. 3BP-LCNP-FA is injected into the blood stream by intraperitoneal injection, and the drug is transported into tumor cells based on the enhanced permeability and retention effect and folate receptor-mediated endocytosis. After local release of the drug, hexokinase on the mitochondria can inhibit the ATP acquisition of tumor cells and cause cell death without affecting normal cells. (The following images represent three independent experiments).

for *in vitro* evaluation. CNE-ZZ cells were maintained at 5% CO<sub>2</sub> and 37°C in 1640 medium supplemented with 1% penicillin and streptomycin and 10% fetal bovine serum. MDA-MB-231 cells were maintained at 5% CO<sub>2</sub> and 37°C in Dulbecco's modified Eagle's medium supplemented with 1% penicillin and streptomycin and 15% fetal bovine serum. BALB/C nude mice were purchased from the Cavens lab animal company (Jiangsu, China) and housed in a laboratory free of specific pathogen barriers in plastic cages with sealed air filtration devices. Feed, litter, and water were all aseptically treated. The temperature was maintained at 26–28°C and the relative humidity was maintained at 40–60%. The light and dark periods were 10 h and 14 h per day, respectively.

### Synthesis and characterization of FA-conjugated F127

To construct cubosomes capable of targeting FRs in tumor cells, we modified F127 with FA (F127-FA), which was prepared according to previously reported methods [31]. Following activation of the amino terminus of FA, we coupled FA to F127 through an amidation reaction on the terminal carboxyl group of F127. The overall process involved dissolving 87.58 mg of FA in 5 mL of dry dimethyl sulfoxide (DMSO), which was then

stirred until complete dissolution. Then, 35.32 mg of CDI was mixed, and the reaction was magnetically stirred for 24 h in the dark. Subsequently, 0.62 g of F127 was added to the solution and the reaction was placed in the dark for 24 h. All reactions were conducted at 25°C. The reaction mixture was transferred into a dialysis bag and dialyzed for 3 days against double-steaming water, which was changed every 3–6 h. F127-FA was recovered via lyophilization. The resulting product was dried in a vacuum oven for 24 h and stored in a dry box until use. Differential scanning calorimetry was conducted to pre-evaluate the conjugated F127-FA. The synthesized F127-FA was dissolved in DMSO to record a spectrum using proton nuclear magnetic resonance (<sup>1</sup>H-NMR) spectroscopy (600 MHz).

### Preparation and characterization of cubosomes

3BP-LCNP and 3BP-LCNP-FA were prepared using an injection method combined with high-pressure homogenization. Briefly, GMO and FA/F127-FA were melted in a water bath at 60°C, followed by the addition of 3BP. After melting, deionized water was slowly added dropwise to obtain a crude solution. This solution was then passed through a high-pressure homogenizer (14,900 psi, nine cycles). During the preparation, 3BP-LCNP

used F127 without FA modification. The sample volume was approximately 10 mL and consisted of approximately 96.1 wt% water, 3.5 wt% GMO, and 0.4 wt% F127-FA. Drug loading was approximately  $1.07 \times 10^{-3}$  wt%. The crystallinity phenomenon of 3BP-LCNP and 3BP-LCNP-FA was observed via polarized light microscopy (PLM), wherein ordinary light is converted into polarized light for microscopy. A substance can be identified as a single refractive (isotropy) or birefringence (anisotropy) structure based on its optical properties; moreover, the crystal form of the object can be quickly and accurately observed. PLM can also be used to observe the crystal structure of cubic liquid crystal. Cubosomes are optically isotropic and exhibit a dark field of vision by PLM. In addition, size distributions of 3BP-LCNP and 3BP-LCNP-FA were assessed using Zeta Sizer Nano series Nano-ZS (Malvern Instruments Ltd., Malvern, UK). Characterization of 3BP-LCNP-FA particle morphology was performed using transmission electron microscopy.

### Evaluation of encapsulation efficiency

Encapsulation efficiencies (EE) of 3BP-LCNP and 3BP-LCNP-FA were determined by dialysis. First, 5 mL of sample was added into a dialysis bag and stirred for 4 h in 200 mL double-distilled water. The concentration of 3BP was determined inside and outside the dialysis bag by using high-performance liquid chromatography. The calculation formula of entrapment efficiency (EE%) is  $EE\% = (C_t - C_p) / C_t \times 100\%$  where  $C_t$  is the total concentration of 3BP in the cubosomes and  $C_p$  is the concentration of 3BP in the dialysis fluid.

### 3BP and 3BP-LCNP-FA release *in vitro*

*In vitro* drug release of 3BP and 3BP-LCNP-FA was determined by dialysis. In brief, 3BP and 3BP-LCNP-FA (5 mL each) were added to dialysis bags and placed in a phosphate solution medium (pH 6.8, tumor microenvironment). At different time intervals, 1 mL of dialysate was removed and replaced with the same amount of fresh phosphate-buffered saline (PBS) supplemented solution (pH 6.8). Free 3BP content in each dialysate was determined by high-performance liquid chromatography using a 204-nm ultraviolet detector and a C18-alkyl reverse phase bonded column. The mobile phase was a 9: 1 mixture of 0.1% trifluoroacetic acid aqueous solution and 0.1% trifluoroacetic acid acetonitrile solution. The flow rate was 1 mL/min, and the elution time was 8 min.

### Morphological changes in cells

To observe changes in cell and nucleus morphology following treatment with different dosage forms of 3BP, CNE-ZZ ( $2.5 \times 10^3$ ) and MDA-MB-231 ( $3.5 \times 10^3$ ) cells were seeded into six-well plates. When the cells covered approximately 70% of the plate bottom, different dosage forms of 3BP were

administered (with a constant 3BP concentration of 50  $\mu$ M). After 24 h, the dead cells in the culture medium were washed off with PBS, and the remaining cells were fixed with 4% paraformaldehyde for 30 min. Paraformaldehyde was then washed off with PBS and 4',6-diamidino-2-phenylindole was added for staining for 15 min. After staining, 4',6-diamidino-2-phenylindole was washed off with PBS, and the morphological changes of cells and cell density were observed using a live cell workstation after adding PBS.

### Cytotoxicity *in vitro*

For cytotoxicity testing, healthy CNE-ZZ ( $5 \times 10^3$ ) and MDA-MB-231 ( $8 \times 10^3$ ) cells were seeded in 96-well plates for 24 h. When cell density reached approximately 70%, the cell culture medium was replaced with a drug-containing medium including different concentrations of LCNP-FA, 3BP, 3BP-LCNP, or 3BP-LCNP-FA (with a consistent 3BP concentration of 50  $\mu$ mol/L). After further incubation for 24 h, cell viability was determined using a 3-(4,5-dimethylthiazol-2-yl)-2,5-diphenyltetrazolium bromide assay.

### Intracellular ATP levels

The ATP level in cells was measured using the ATP assay kit. CNE-ZZ ( $2.5 \times 10^5$ ) and MDA-MB-231 ( $3.5 \times 10^5$ ) cells were seeded in six-well plates and cultured for 24 h. LCNP-FA-, 3BP-, 3BP-LCNP-, or 3BP-LCNP-FA-containing culture medium was then added to the cells for 4 and 6 h at 37°C.

### Animal experiments

BALB/C nude mice (4 to 5 weeks old, female) bearing tumors were established by inoculating  $5 \times 10^6$  CNE-ZZ cells into the right flank. To evaluate the targeted therapeutic effect of 3BP-LCNP-FA *in vivo*, the mice were divided into five groups (control, LCNP-FA, 3BP, 3BP-LCNP, and 3BP-LCNP-FA) of four mice each. When the tumor grew (volume = length  $\times$  width<sup>2</sup>/2) to approximately 70 mm<sup>3</sup>, the different groups (with a constant 3BP concentration of 8 mg/kg and injection volume of 0.1 mL/mouse) were injected intraperitoneally with the respective drug formulations. After dosing every other day for 2 weeks, tumor volumes were compared to evaluate the targeted antitumor effect *in vivo*. Changes in body weight of nude mice were used to evaluate the toxicity of different drug formulations. Two days after the final treatment, the mice were euthanized by cervical dislocation. Tumors from all the mice were extracted and weighed for comparison of treatment effects. Serum was collected for assessment of liver and kidney toxicity; organs (the kidney, lung, and liver) were excised for histopathological examination using hematoxylin and eosin staining. Proliferation of tumor tissue was observed via proliferating cell nuclear antigen (PCNA) immunohistochemistry and

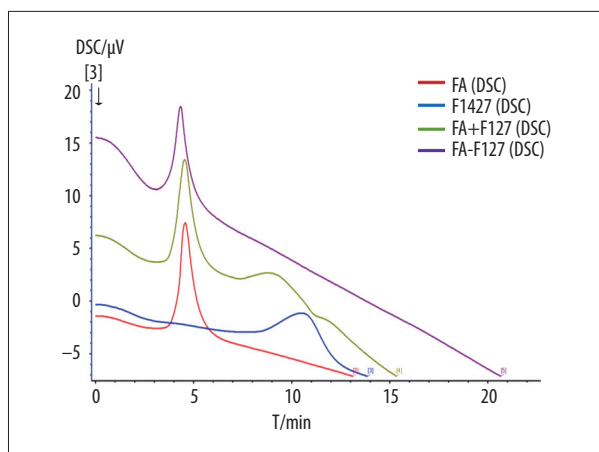


**Figure 2.** Differential scanning calorimetry characterization of FA-F127.

tumor tissue apoptosis was evaluated using a terminal deoxynucleotidyl transferase dUTP nick end labeling (TUNEL) assay.

### Statistical analysis

All experiments were performed independently and repeated at least three times. Statistical comparisons of data sets were

evaluated using the Student's *t*-test and one-way analysis of variance test.  $P < 0.05$  was considered statistically significant.

## Results

### Characterization of FA-conjugated F127

Conjugation of FA and F127 was evaluated using differential scanning calorimetry (Figure 2). The purple curve representing F127-FA lacked the characteristic absorption peak of FA, indicating that F127-FA was a single compound. The <sup>1</sup>H-NMR spectrum of F127-FA showed absorbance peaks corresponding to the following components: 1.01 (CH<sub>3</sub> in PPO of F127), 3.44–3.51 (CH in PPO of F127), 3.53 (CH<sub>2</sub>CH<sub>2</sub>O of F127), 6.6 and 7.6 (3,5-H and 2,6-H of the FA benzene ring), and 8.6 (C7-H in the FA pteridine proton) (Figure 3).

### Characterization of cubosomes

The results showed that cubosomes were prepared when GMO: F127 was 8: 1 (by% of weight, with a consistent total mass of 1 g). Consistent with the optical isotropy exhibited by cubosomes, we observed 3BP-LCNP as a dark field. Notably,

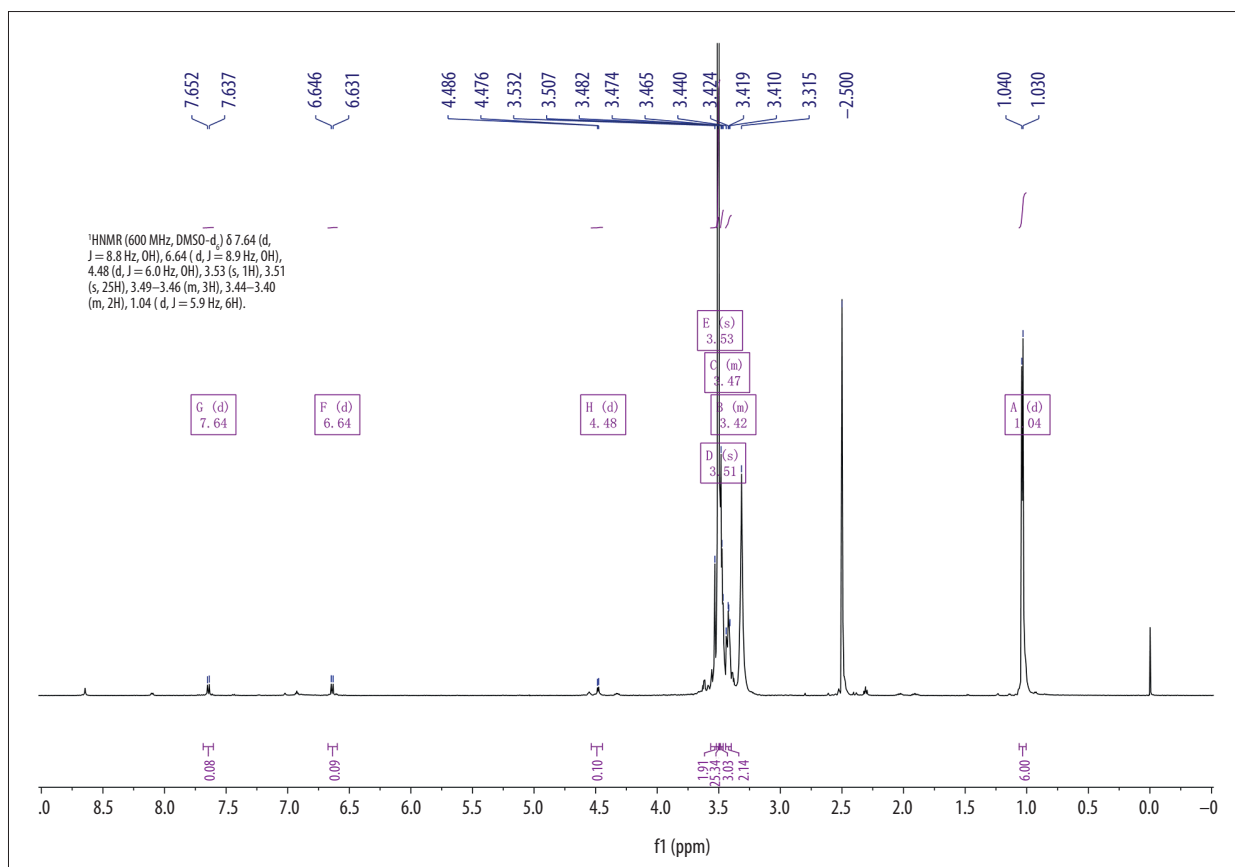


**Figure 3.** <sup>1</sup>H-NMR spectrum of F127-FA.



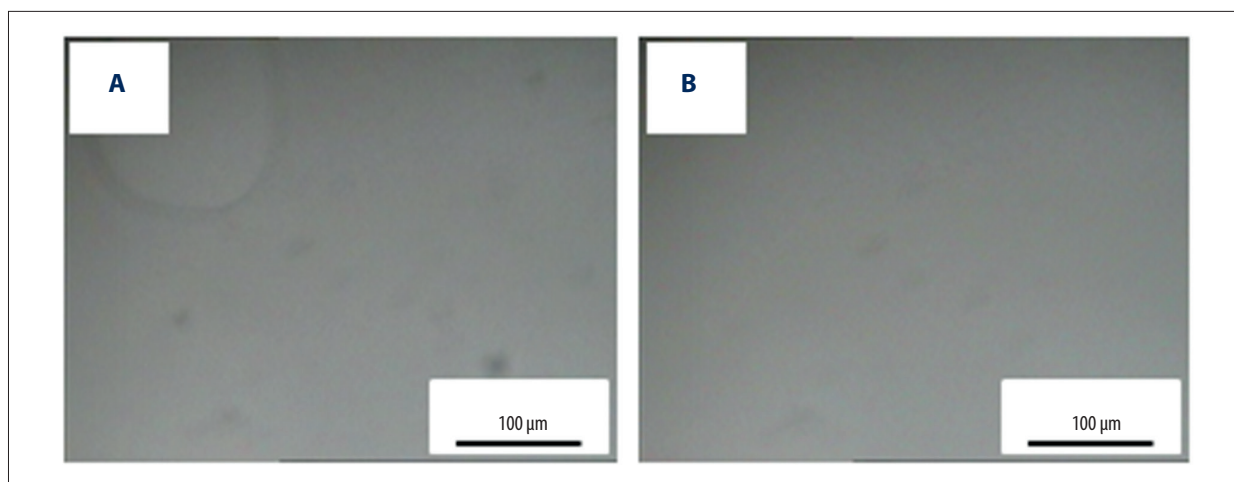


**Figure 4.** PLM characterization of cubosomes. (A) 3BP-LCNP; (B) 3BP-LCNP-FA.

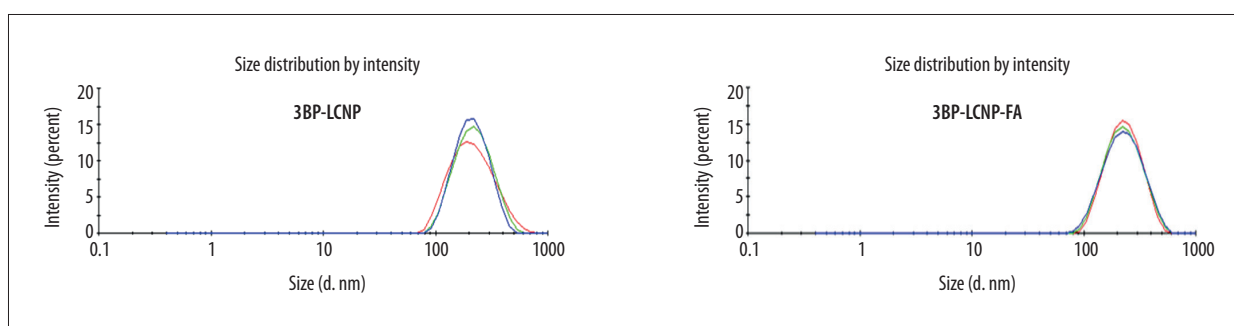


**Figure 5.** Size and PDI distribution of 3BP-LCNP and 3BP-LCNP-FA. Different colors represent three tests (n=3).

**Table 1.** Average size and polydispersity index of 3BP-LCNP and 3BP-LCNP-FA (n=3).

Sample	Average size	PDI
3BP-LCNP	192.3	0.113
3BP-LCNP-FA	201.7	0.102

3BP-LCNP-FA still appeared as a dark field following drug loading (Figure 4A, 4B), indicating that drug loading did not affect the morphology of the prepared liquid crystal.

Homogenization at 14,900 psi for nine cycles yielded an adequate particle size. The addition of FA increased the average particle size from 192.3 to 201.7 nm and the polydispersity index (PDI) decreased from 0.113 to 0.102 (Figure 5, Table 1). The EE of the prepared 3BP-LCNP-FA was around 70.23%. Figure 6 shows the structure of 3BP-LCNP-FA under a cryo-projective electron microscope; spherical particles of uniform size that were not adherent to each other were observed.

### 3BP-LCNP-FA release profile *in vitro*

Release of 3BP at drug concentrations of 5, 10, 25, 50, 90, 100, 250, and 500 μg/mL from 3BP-LCNP-FA showed a linear profile. Free 3BP exhibited almost 100% release within 3 h. In comparison, only 90.79% of 3BP was released from 3BP-LCNP-FA within 48 h (Figure 7), indicating that 3BP-LCNP-FA presented a slower drug release pattern than free 3BP.

### Morphological changes in cells

The blank vector LCNP-FA had no significant effect on the morphology or density of CNE-ZZ and MDA-MB-231 cells ( $P > 0.05$ ) (Figure 8A, 8B). The effects of 3BP, 3BP-LCNP, and 3BP-LCNP-FA on the morphology and density of CNE-ZZ cells were similar ( $P > 0.05$ ). Morphology and density of MDA-MB-231 cells were not significantly changed by 3BP ( $P > 0.05$ ). In contrast, 3BP-LCNP and 3BP-LCNP-FA significantly reduced the density of MDA-MB-231 cells ( $P < 0.01$ ) and caused changes in nuclear morphology, including gradual condensation of chromatin into a crescent shape and attachment to the periphery of the nuclear membrane; nuclear envelope breakdown; and nuclear division. However, the cell membrane remained intact.

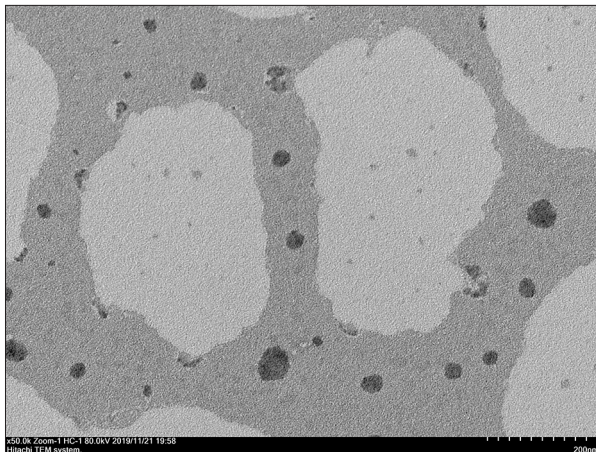


Figure 6. TEM characterization of 3BP-LCNP-FA.

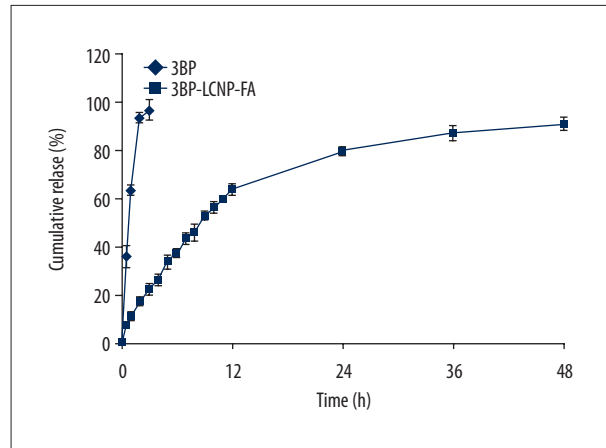


Figure 7. *In vitro* release of 3BP and 3BP-LCNP-FA (pH 6.8). Data represent the mean±S.D. of three independent experiments.

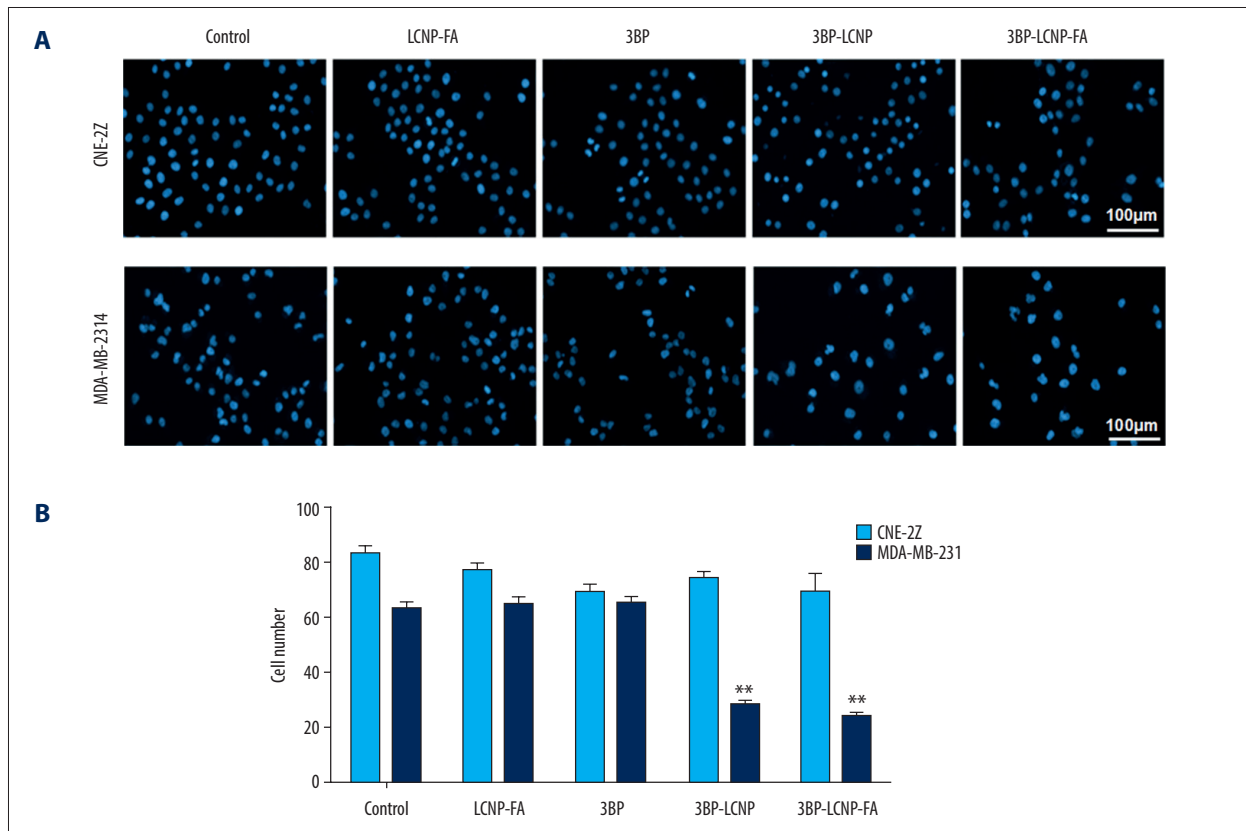
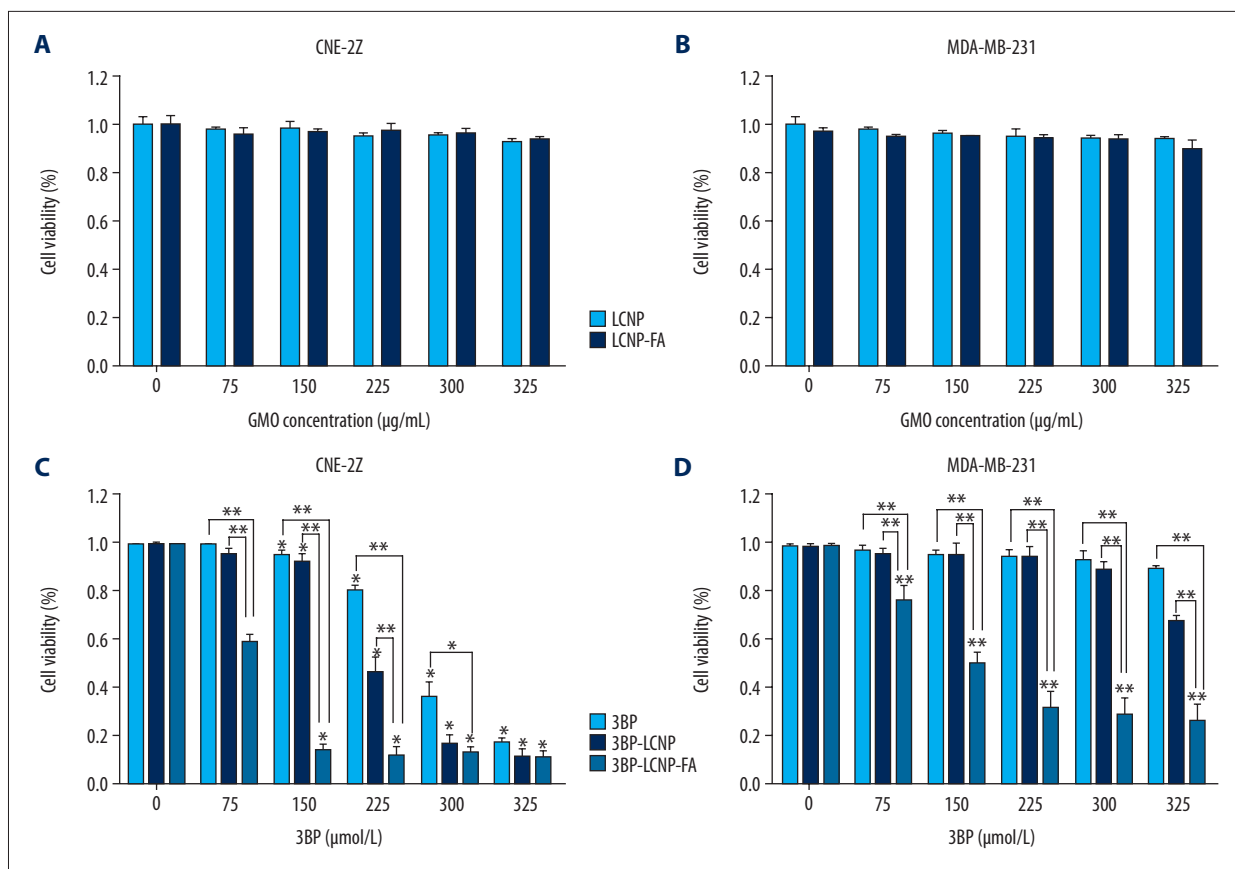


Figure 8. (A) Cell morphology changes and (B) cell density changes after LCNP-FA, 3BP, 3BP-LCNP, and 3BP-LCNP-FA treatment.

### Inhibitory effect of 3BP-LCNP-FA on tumor cell proliferation

To elucidate the effects of 3BP-LCNP-FA on tumor cells, we evaluated the proliferation of CNE-ZZ and MDA-MB-2314 cells after treatment. As shown in Figure 9A and 9B, increasing doses of the empty vectors LCNP and LCNP-FA had no significant

inhibitory effects on proliferation in either cell line after 24 h. However, in CNE-ZZ cells, 50  $\mu$ M of 3BP-LCNP-FA caused 86.3% inhibition in proliferation, whereas 3BP and 3BP-LCNP caused 7.8% and 4.6% inhibition, respectively (Figure 9C). As 3BP drug concentrations increased, the inhibition rate reached over 80% at 125  $\mu$ M. In contrast, as can be seen in Figure 9D, increasing concentrations of 3BP did not significantly inhibit



**Figure 9.** Cytotoxicity of different drug formulations in CEN2Z and MDA-MB-231 cells by MTT. (A) Blank vectors LCNP and LCNP-FA on CNE-2Z and (B) MDA-MB-231. (C) 3BP, 3BP-LCNP, 3BP-LCNP-FA on CNE-2Z and (D) MDA-MB-231. Data are representative of three separate experiments with similar results. \* P<0.05, \*\* P<0.01.

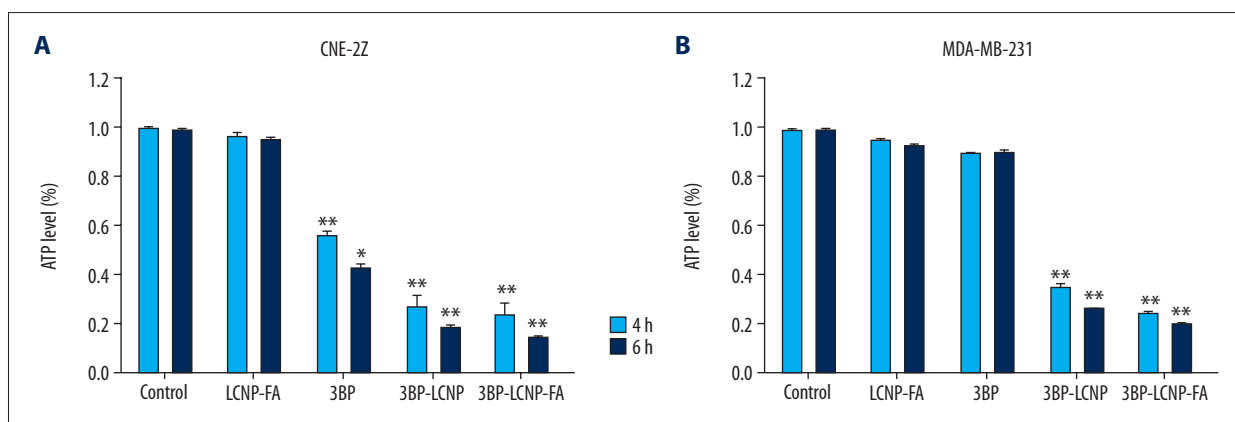


**Figure 10.** (A) Changes in intracellular ATP levels after 4 and 6 h of LCNP-FA, 3BP, 3BP-LCNP, and 3BP-LCNP-FA treatment on CNE-2Z and (B) MDA-MB-231 cells. Data represent the mean±S.D. of three independent experiments, \* P<0.05, \*\* P<0.001.

cell proliferation in MDA-MB-231 cells; e.g., when 3BP concentration reached 125 µM, the inhibition rate was only 10.2%. In comparison, the inhibitory rate of 3BP-LCNP-FA reached 50.2% at 50 µM, with the inhibitory effect increasing with increased drug concentration.

### Changes in intracellular ATP levels

Figure 10 shows changes in intracellular ATP levels in CNE-2Z and MDA-MB-231 cells after the different drug delivery forms were administered for 4 and 6 h. Intracellular ATP levels in MDA-MB-231 cells did not decrease significantly with increased



3BP concentration, and no significant difference was observed compared with that in the control group ( $P>0.05$ ). In contrast, ATP levels in 3BP-, 3BP-LCNP-, and 3BP-LCNP-FA-treated cells showed a significant decrease compared with that in the control group ( $P<0.05$ ).

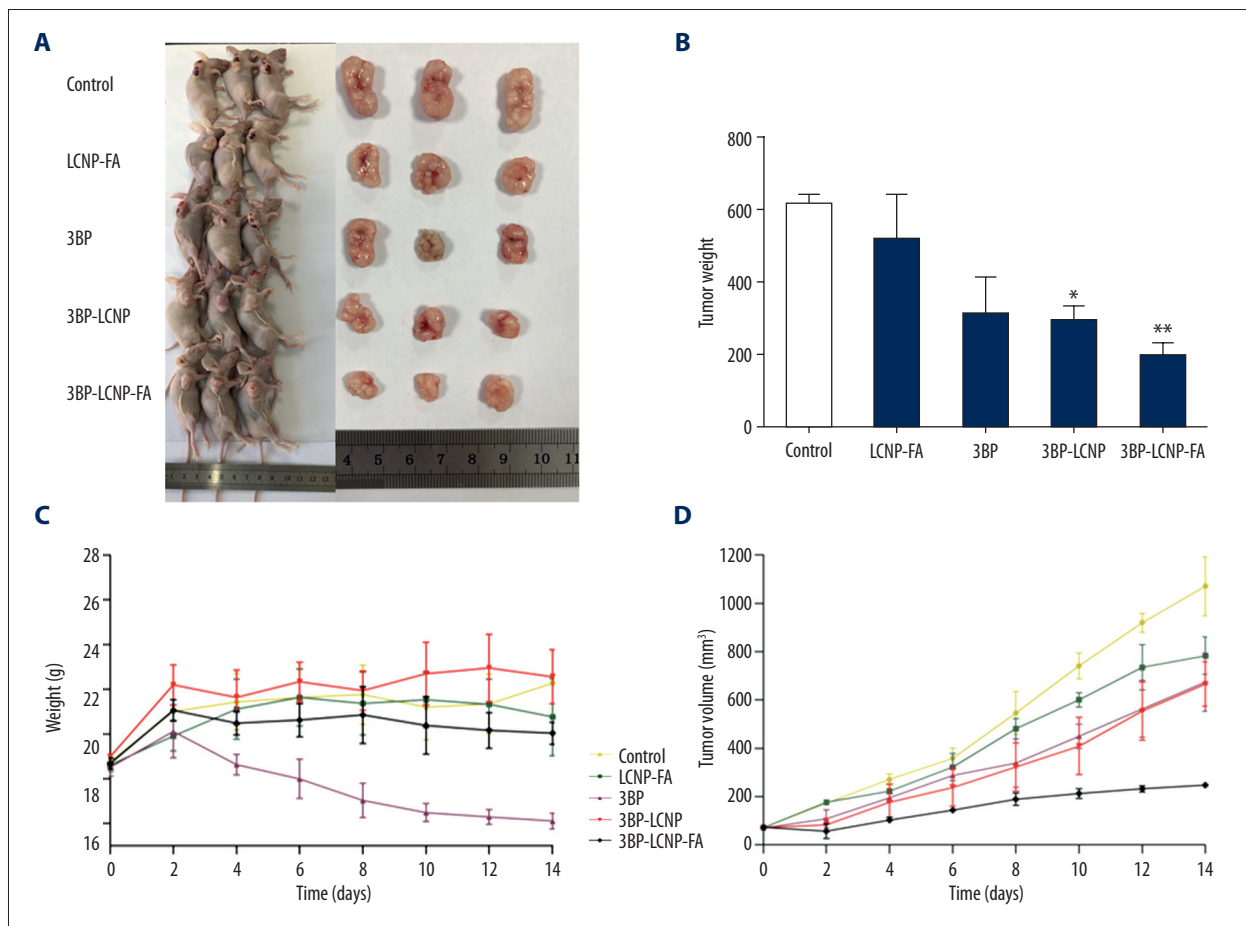
### Results of 3BP-LCNP-FA treatment *in vivo*

Tumor volume is the most effective parameter for evaluating the therapeutic effect of a drug in tumor-bearing nude mice. Tumor volume in different dosage groups (Figure 11A) and results of tumor weight analyses (Figure 11B) revealed that both 3BP-LCNP and 3BP-LCNP-FA exhibited significant inhibitory effects on tumor growth ( $P<0.05$ ). During the treatment period, the body weight of nude mice in the 3BP administration group showed a downward trend, which was not observed in the other groups (Figure 11C). Evaluation at different time points during administration revealed that tumor volume in the 3BP administration group increased from 70 to approximately 678  $\text{mm}^3$ , whereas in the 3BP-LCNP-FA treatment group, it increased to only 248  $\text{mm}^3$  (Figure 11D). Tumor growth was inhibited more significantly by 3BP-LCNP-FA than by LCNP-FA/3BP/3BP-LCNP, with no obvious toxic and side effects. Hematoxylin and eosin-stained

sections of the liver, kidney, lung, and tumor from the different groups revealed no obvious morphological changes in any of the observed tissues (Figure 11E). Analysis of markers related to organ damage indicated that levels of alanine transaminase (ALT), aspartate aminotransferase (AST), creatinine (Cr), and blood urea nitrogen (BUN) in the treatment groups were within the normal range (Figure 11F). The result of PCNA immunohistochemistry showed that PCNA was localized in the nucleus; the positive markers (HRP-DAB/ $\text{H}_2\text{O}_2$ ) appeared as light-yellow and brown-yellow granules (Figure 11G). The highest PCNA expression was observed in 3BP-LCNP-FA-treated mice, followed by (in order) those treated with 3BP-LCNP, 3BP, LCNP-FA, and control. Results of the TUNEL assay used to observe the extent of apoptosis in the tumor tissues revealed the highest expression level of green particles in tumors from 3BP-LCNP-FA-treated mice, followed by (in order) those from mice treated with 3BP-LCNP, 3BP, LCNP-FA, and control (Figure 11H).

### Discussion

In the process of preparation, cubosomes will form a lipid bilayer structure and then extend in three-dimensional space



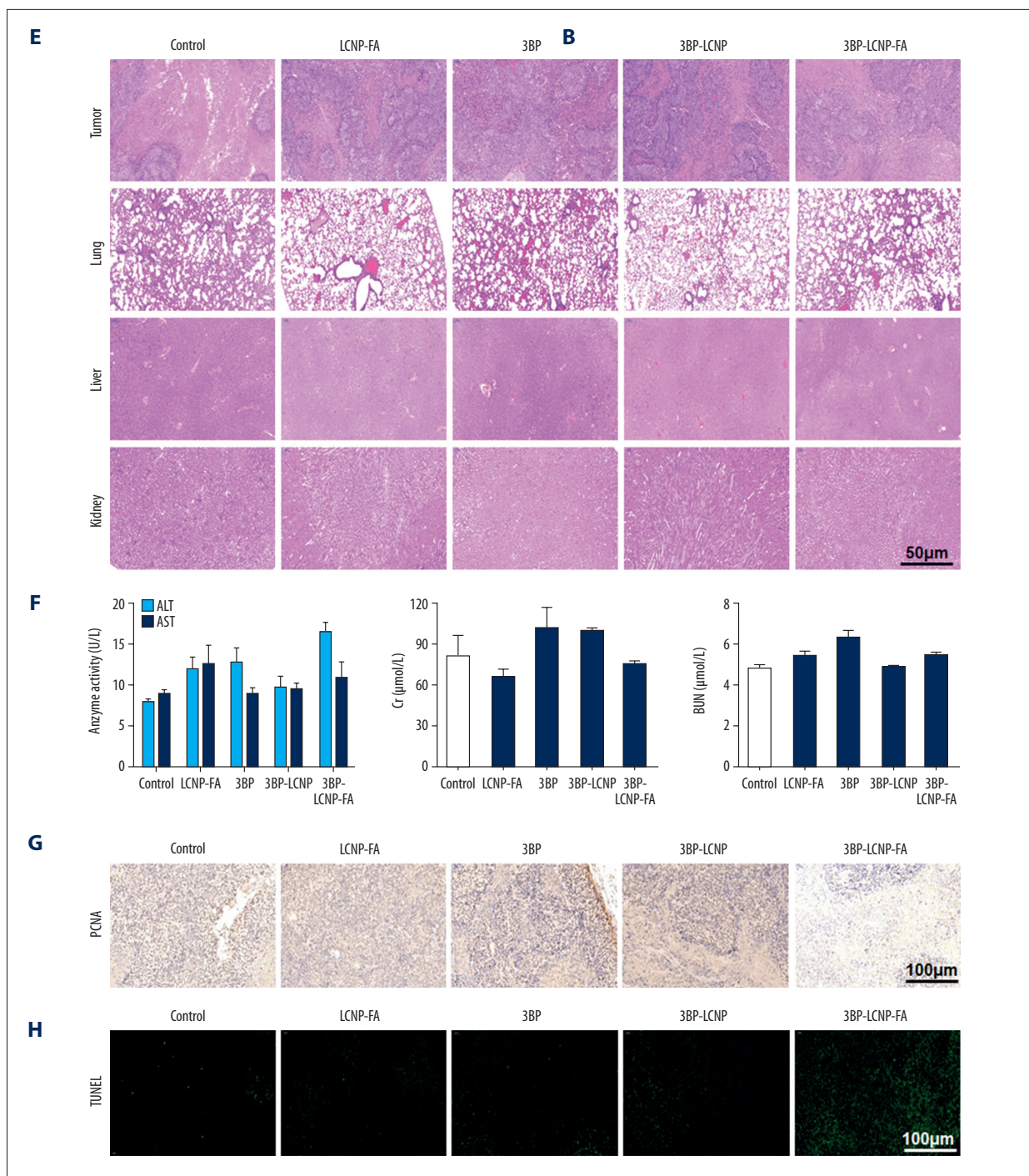


**Figure 11.** Antitumor activity evaluation of 3BP-LCNP-FA *in vivo*. (A) Formation of tumors in control, LCNP-FA, 3BP, 3BP-LCNP, and 3BP-LCNP-FA groups of mice. After nude mice were sacrificed in the last administration, tumor weights of different dosage groups were analyzed. (B) Data are presented as mean±S.D. (n=4) \* P<0.05, \*\* P<0.01. (C) Change curves of mice weight and (D) tumor volume were measured at different time points after administration of different dosage forms. Data are presented as mean±S.D. (n=4). H & E staining of the tumors, lung, liver, and kidney after LCNP-FA, 3BP, 3BP-LCNP, and 3BP-LCNP-FA treatment vs. control. (E) The images are representative of three independent experiments. After LCNP-FA, 3BP, 3BP-LCNP, and 3BP-LCNP-FA treatment, the levels of AST, ALT, Cr, and BUN were evaluated by taking orbital venous blood. (F) Data represent the Mean±S.D. (n=6). PCNA immunohistochemistry of LCNP, 3BP, 3BP-LCNP, and 3BP-LCNP-FA treatment. (G) The images are representative of three independent experiments. TUNEL assay of LCNP, 3BP, 3BP-LCNP, and 3BP-LCNP-FA treatment. (H) The images are representative of three independent experiments.

to form a compact and stable cubic liquid crystal system with various structures, in which the smallest lattice is a cube [32]. Because cubosomes are a self-stable system, they are superior to traditional nanocarrier systems, such as micelles and liposomes. Although cubosomes have been shown to exhibit strong antitumor effects *in vitro*, evaluation of their antitumor effects and drug toxicity *in vivo* is more relevant to ultimate clinical application [18]. For example, some studies have reported that cubosomes are not stable in blood. When cubosomes come in contact with plasma, the liquid crystal structure changes and affects drug release. However, cubosomes can still increase the action time of a drug through circulation in the body. For example, the addition of poloxamer 407 in the preparation of cubosomes can further stabilize the spatial structure of the particles. Nonetheless, whether the particle structure of 3BP-LCNP-FA remains intact for the desired time after a stabilizer is added remains to be further investigated based on the targeting afforded by the enhanced permeability and retention effect and FA-FR to the tumor site. In this study, we observed that the antitumor effect of 3BP-LCNP-FA was superior to those of 3BP-LCNP and 3BP. Nevertheless, the specific phase transition mechanism of cubic liquid crystal in blood, such as the effects of plasma ionomer, microenvironment, and organelle, remains to be further studied.

In the current study, we also evaluated levels of markers associated with organ damage. Specifically, ALT, which is present in the cytoplasm of hepatocytes, and AST, which is mainly present in the cytoplasm and mitochondria of hepatocytes, are released into the blood during cell degeneration, membrane necrosis, cell permeability, or membrane damage. BUN and Cr are markers of renal injury. Notably, these levels were all within normal ranges, suggesting that 3BP-LCNP-FA exhibited no hepatotoxicity or nephrotoxicity. In addition, absence of morphological changes indicated no significant toxicity or

side effects in the liver, kidney, or lung in each treatment group. TUNEL assay results further demonstrated that 3BP-LCNP-FA inhibited tumor cell proliferation and increased tumor apoptosis, implying its potent inhibitory effects on tumor growth. Overall, these results indicated that it is feasible to enhance the efficacy of antitumor drugs by modifying the drug delivery system. The results of this study, therefore, may have promising implications for future 3BP research and clinical application.

This study has several potential limitations. The antitumor effect of 3BP-LCNP-FA was greater than that of LCNP-FA/3BP/3BP-LCNP based on pharmacodynamics. However, the specific mechanisms of action have not been clarified, including accurate details regarding the tumor targeting and release mechanism in cells after 3BP-LCNP-FA enters the blood. Follow-up experiments will be required to evaluate the precise modes of action and antitumor effects of 3BP-LCNP-FA from the perspective of molecular mechanisms.

## Conclusions

In this study, the performance of a prepared drug delivery platform was evaluated using PLM, differential scanning calorimetry, and <sup>1</sup>H-NMR spectroscopy. 3BP-LCNP-FA can be successfully constructed as a drug delivery vehicle that has no obvious toxic effects *in vivo*. Our findings show that a cubic liquid crystal modified by FA can be used as an effective carrier for targeted 3BP administration.

## Acknowledgements

We would like to thank Editage ([www.editage.cn](http://www.editage.cn)) for English language editing.

## References:

1. Warburg O: On the origin of cancer cells. *Science*, 1956; 123(3191): 309–14
2. Gonzalez CD, Alvarez S, Ropolo A et al: Autophagy, Warburg, and Warburg reverse effects in human cancer. *BioMed Res Int*, 2014; 2014: 926729
3. Xian SL, Cao W, Zhang XD, Lu YFL 3-Bromopyruvate inhibits human gastric cancer tumor growth in nude mice via the inhibition of glycolysis. *Oncol Lett*, 2015; 9(2): 739–44
4. Ganapathy-Kanniappan S, Vali M, Kunjithapatham R et al: 3-Bromopyruvate a new targeted antiglycolytic agent and a promise for cancer therapy. *Curr Pharm Biotechnol*, 2010; 11(5): 510–17
5. El Sayed SM, Mahmoud AA, El Sawy SA et al: Warburg effect increases steady-state ROS condition in cancer cells through decreasing their antioxidant capacities (anticancer effects of 3-bromopyruvate through antagonizing Warburg effect). *Med Hypotheses*, 2013; 81(5): 866–70
6. Cardaci S, Desideri E, Ciriolo MR: Targeting aerobic glycolysis: 3-bromopyruvate as a promising anticancer drug. *J Bioenerg Biomembr*, 2012; 44(1): 17–29
7. Pan Q, Sun Y, Jin Q et al: Hepatotoxicity and nephrotoxicity of 3-bromopyruvate in mice. *Acta Cir Bras*, 2016; 31(11): 724–29
8. Lis P, Zarzycki M, Ko YH et al: Transport and cyto toxicity of the anticancer drug 3-bromopyruvate in the yeast *Saccharomyces cerevisiae*. *J Bioenerg Biomembr*, 2012; 44(1): 155–61
9. Azevedo-Silva J, Queiros O, Baltazar F et al: The anticancer agent 3-bromopyruvate: A simple but powerful molecule taken from the lab to the bedside. *J Bioenerg Biomembr*, 2016; 48(4): 349–62
10. Yadav S, Kujur PK, Pandey SK et al: Antitumor action of 3-bromopyruvate implicates reorganized tumor growth regulatory components of tumor milieu, cell cycle arrest and induction of mitochondria-dependent tumor cell death. *Toxicol Applied Pharmacol*, 2018; 339: 52–64
11. Gong L, Wei Y, Yu X et al: 3-bromopyruvic acid, a hexokinase ii inhibitor, is an effective antitumor agent on the hepatoma cells: *In vitro* and *in vivo* findings. *Anticancer Agents Med Chem*, 2014 14(5): 771–76
12. Pedersen PL: 3-bromopyruvate (3BP) a fast acting, promising, powerful, specific, and effective “small molecule” anti-cancer agent taken from lab-side to bedside: Introduction to a special issue. *J Bioenerg Biomembr*, 2012; 44(1): 1–6
13. Yadav S, Pandey SK, Goel Y et al: Diverse Stakeholders of tumor metabolism: An appraisal of the emerging approach of multifaceted metabolic targeting by 3-bromopyruvate. *Frontiers Pharmacol*, 2019; 10: 728

14. Zou X, Zhang M, Sun Y et al: Inhibitory effects of 3-bromopyruvate in human nasopharyngeal carcinoma cells. *Oncol Rep*, 2015; 34(4): 1895–904
15. Azevedo-Silva J, Queiros O, Ribeiro A et al: The cytotoxicity of 3-bromopyruvate in breast cancer cells depends on extracellular pH. *Biochem J*, 2015; 467(2): 247–58
16. El Sayed SM, Baghdadi H, Zolaly M et al: The promising anticancer drug 3-bromopyruvate is metabolized through glutathione conjugation which affects chemoresistance and clinical practice: An evidence-based view. *Med Hypotheses*, 2017; 100: 67–77
17. Glick M, Biddle P, Jantzi J et al: The antitumor agent 3-bromopyruvate has a short half-life at physiological conditions. *Biochem Biophys Res Commun*, 2014; 452(1): 170–73
18. Ko YH, Verhoeven HA, Lee MJ et al: A translational study “case report” on the small molecule “energy blocker” 3-bromopyruvate (3BP) as a potent anticancer agent: From bench side to bedside. *J Bioenerg Biomembr*, 2012; 44(1): 163–70
19. Sadowska-Bartosz I, Szewczyk R, Jaremko L et al: Anticancer agent 3-bromopyruvic acid forms a conjugate with glutathione. *Pharmacol Rep*, 2016; 68(2): 502–5
20. El Sayed SM, Mohamed WG, Seddik MA et al: Safety and outcome of treatment of metastatic melanoma using 3-bromopyruvate: A concise literature review and case study. *Chin J Cancer*, 2014; 33(7): 356–64
21. Qiao J, Dong P, Mu X et al: Folic acid-conjugated fluorescent polymer for up-regulation folate receptor expression study via targeted imaging of tumor cells. *Biosens Bioelectron*, 2016; 78: 147–53
22. Hartmann LC, Keeney GL, Lingle WL et al: Folate receptor overexpression is associated with poor outcome in breast cancer. *Int J Cancer*, 2007; 121(5): 938–42
23. Leamon CP: Folate-targeted drug strategies for the treatment of cancer. *Curr Opin Investig Drugs*, 2008; 9(12): 1277–86
24. Segal EI, Low PS: Tumor detection using folate receptor-targeted imaging agents. *Cancer Metastasis Rev*, 2008; 27(4): 655–64
25. Park EK, Kim SY, Lee SB, Lee YM: Folate-conjugated methoxy poly(ethylene glycol)/poly(epsilon-caprolactone) amphiphilic block copolymeric micelles for tumor-targeted drug delivery. *J Controlled Release*, 2005; 109(1–3): 158–68
26. Luzzati V, Tardieu A, Gulik-Krzywicki T et al: Structure of the cubic phases of lipid-water systems. *Nature*, 1968; 220(5166): 485–88
27. Luzzati V, Vargas R, Mariani P et al: Cubic phases of lipid-containing systems. Elements of a theory and biological connotations. *J Mol Biol*, 1993; 229(2): 540–51
28. Chountoules M, Pippa N, Pispas S et al: Cubic lyotropic liquid crystals as drug delivery carriers: Physicochemical and morphological studies. *Int J Pharm*, 2018; 550(1–2): 57–70
29. Madheswaran T, Kandasamy M, Bose RJ, Karuppagounder V: Current potential and challenges in the advances of liquid crystalline nanoparticles as drug delivery systems. *Drug Discovery Today*, 2019; 24(7): 1405–12
30. Zhai J, Fong C, Tran N, Drummond CJ: Non-lamellar lyotropic liquid crystalline lipid nanoparticles for the next generation of nanomedicine. *ACS Nano*, 2019; 13(6): 6178–206
31. Butt AM, Mohd Amin MC, Katas H: Synergistic effect of pH-responsive folate-functionalized poloxamer 407-TPGS-mixed micelles on targeted delivery of anticancer drugs. *Int J Nanomed*, 2015; 10: 1321–34
32. Li J, Wu L, Wu W et al: A potential carrier based on liquid crystal nanoparticles for ophthalmic delivery of pilocarpine nitrate. *Int J Pharm*, 2013; 455(1–2): 75–84